Laser and Particle Beams (2008), *26*, 583–589. Printed in the USA.

doi:10.1017/S0263034608000645

Temperature measurement of warm-dense-matter generated by intense heavy-ion beams

P.A. NI,[1] M.I. KULISH,[2] V. MINTSEV,[2] D.N. NIKOLAEV,[2] V.YA. TERNOVOI,[2] D.H.H. HOFFMANN,[3] S. UDREA,[3] A. HUG,[4] N.A. TAHIR,[4] AND D. VARENTSOV[4]

[1]Lawrence Berkeley National Laboratory, University of California, Berkeley, California
[2]Institute of Problems of Chemical Physics, Chernogolovka, Russia
[3]Institut für Kernphysik, Technische Universität Darmstadt, Darmstadt, Germany
[4]Gesellschaft für Schwerionenforschung mbH, Darmstadt, Germany

(RECEIVED 19 May 2008; ACCEPTED 25 September 2008)

Abstract

This paper describes a fast multi-channel radiation pyrometer that was developed for warm dense-matter experiments with intense heavy ion beams at the Gesellschaft für Schwerionenforschung mbH (GSI). The pyrometer is capable of measuring brightness temperatures from 2000 K to 50,000 K, at six wavelengths in the visible and near-infrared parts of the spectrum, with 5 ns temporal resolution, and several micrometers spatial resolution. The pyrometer's spectral discrimination technique is based on interference filters, which also act as mirrors to allow for simultaneous spectral discrimination of the same ray at multiple wavelengths.

Keywords: High energy density physics; Temperature diagnostic; Warm dense matter

INTRODUCTION

Powerful lasers, pulsed, high power electrical discharges, high explosives, gas guns, and intense particle beams from accelerators are commonly used experimental tools to generate high energy density states in matter or warm-dense-matter (WDM) (Fortov *et al.*, 2007; Zou *et al.*, 2006; Zvorykin *et al.*, 2007; Hora, 2007; Tahir *et al.*, 2007*a*; Varentsov *et al.*, 2007; Adonin *et al.*, 2007; Mitchell *et al.*, 1991; Weir *et al.*, 1996). Among these techniques, heavy ion beams are relatively new (Varentsov *et al.*, 2007). However, due to their unique ways of interacting with matter, they open new pathways to generate and to diagnose high energy density matter.

A study of the fundamental properties of WDM is an important subject as it has wide applications to various branches of basic and applied sciences (Cao *et al.*, 2007; Sasaki *et al.*, 2006; Tahir *et al.*, 2003). Experimental study of equation-of-state of WDM is of considerable interest to the fundamental research of thermodynamic and hydrodynamic behavior of dense plasmas. This study will enable one to probe the validity of existing theories on stellar formation and evolution, compressibility of inertial fusion targets, and existing models for strongly coupled high density plasmas (Hoffmann *et al.*, 2007; Logan *et al.*, 2007; Henning, 2004; Tahir *et al.*, 2005*b*; Cao *et al.*, 2007; Deutsch & Popoff, 2006; Sasaki *et al.*, 2006).

The heavy ion synchrotron SIS-18 at Gesellschaft für Schwerionenforschung mbH (GSI) is a unique facility that delivers intense beams of highly energetic heavy ions. Using these heavy ion beams it is possible to heat macroscopic volumes of matter to extreme temperatures and pressures with uniform physical conditions (Tahir *et al.*, 2005*a*, 2007*b*).

Recently, a series of WDM physics experiments with heavy ion beams have been carried out at the high temperature experimental area (HHT) of the plasma physics group at GSI (Varentsov *et al.*, 2003, 2007; Udrea *et al.*, 2007; Becker *et al.*, 2006).

In these experiments, metallic targets of macroscopic volumes were heated uniformly and quasi-isochorically by intense uranium ion beams (Fig. 1), thereby generating high-density, high-entropy states. The heated target material was expanding isentropically, passing through physical states located in the region of the boiling curve, two-phase liquid-gas, and the critical point. The heating beam intensity was 4.4×10^9 $^{238}U^{74+}$ ions with particle energy of 350 MeV/u.

Address correspondence and reprint requests to: P.A. Ni, Lawrence Berkeley National Laboratory, University of California, Berkeley, CA 94720-8201. E-mail: pani@lbl.gov

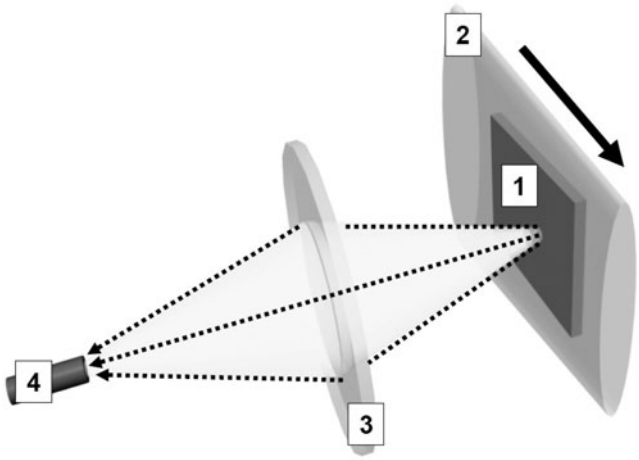

Fig. 1. Schematic layout of experiment: (**1**) target sample, (**2**) focused ion beam with elliptical profile, (**3**) light collection optics capturing sample's thermal radiation, (**4**) optical fiber connected to pyrometer.

The ions were delivered in a single 120 ns bunch (full width at half maximum (FWHM)), resulting in an estimated several kJ/g energy deposition in lead. The thermodynamic properties, i.e., temperature, pressure, expansion velocity, and electrical conductivity, of the target were measured during the heating phase as well as during the expansion phase.

This paper focuses on the six-channel pyrometer developed by scientists from GSI, Technische Universität Darmstadt (TU-Darmstadt), and Institute of Problems of Chemical Physics (IPCP). A pyrometer is a non-contact thermometer, which measures the temperature of an optically thick radiation layer, based on its emitted thermal radiation, while no disturbance of the existing temperature field occurs. The developed instrument measures brightness temperatures at six wavelengths with 5 ns temporal resolution, and a variable spatial resolution of a few 100 μm. The brightness temperatures are obtained from analysis of the Planck radiation in the visible and near-infrared spectral regions (Michalski *et al.*, 2001; Dewitt, 1998). In addition, the absolute radiation emission recorded by the pyrometer at multiple wavelengths gives the possibility for the application of various models of spectral emissivity. In some cases, this leads to a more precise estimation of the physical temperature of the target (Coates, 1988; Pellerin *et al.*, 1992). In the performed WDM experiments, samples of various materials including copper, aluminum, tungsten, tantalum, sapphire, and uranium dioxide, were pulse heated by intense heavy ion beams and temperatures varying from 2000 K to 10,000 K were measured. The different hydrodynamic behavior of these materials is also clearly visible in the pyrometer's records.

PYROMETER

The temporal resolution of the pyrometer suitable for the present experiments with heavy ion beams at GSI is dictated by the 120 ns heating beam duration and therefore must be on a nanosecond scale. A broad working range from 2000 K to 50,000 K is also required since it is desirable to track temperature evolution during all phases of the experiment, which include pulsed heating with the ion beam and consequent cooling due to the free expansion into vacuum.

Light Collection System

Efficient coupling of light into a pyrometer plays an important role and becomes more critical in experiments with lower temperatures (≈2000 K). For WDM experiments at GSI, we have designed a light collection system (condenser), which is compact enough to fit into the target vacuum chamber. At the same time, it has a good efficiency; it is free from chromatic aberrations, having several micrometers spatial resolution. Finally, it matches the 0.22 numerical apertures (NA) of a fused silica, multi-mode fiber, which is used for light coupling into the pyrometer. The thermal radiation is analyzed in the spectral region from 500 nm to 1500 nm. Any condenser built from glass lenses and used in such a broad wavelength range will have chromatic aberrations. This would effectively lead to wavelength dependence of the probing spot size and could be a critical issue in experiments with non-homogenous temperature distribution. In order to exclude chromatic aberrations, two different designs of light collection optics based on spherical and of axis parabolic mirrors were implemented with the principal working scheme explained in Figures 2 and 3.

In both designs, the sample is placed at the focus of the mirror producing a quasi-collimated beam, which is then focused on a fiber array using an identical second mirror. This arrangement produces a quasi 1:1 imaging of the target's surface. The spherical mirrors (200 mm focal length, 80 mm diameter, central through bore 40 mm in diameter, protected silver coating, corrected for coma and spherical aberrations) are a custom product manufactured by Laser Components GmbH (Olching, Germany) using in-house sketches. The parabolic mirrors (101 mm focal length, 50 mm diameter, silver coated) are a standard

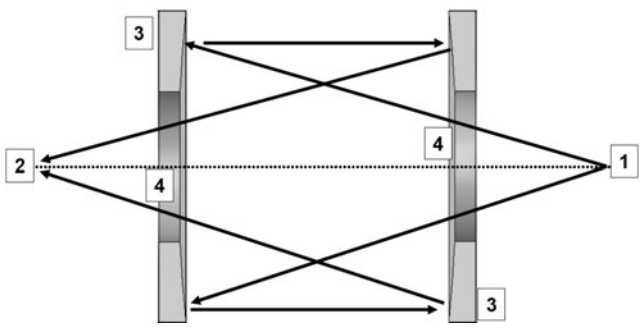

Fig. 2. Working scheme of spherical-mirror-based light collection optics (not to scale), thick lines—show propagation of light in the system: (**1**) position of sample, (**2**) position of optical fiber, (**3**) spherical mirrors, (**4**) central through bore.

https://doi.org/10.1017/S0263034608000645 Published online by Cambridge University Press

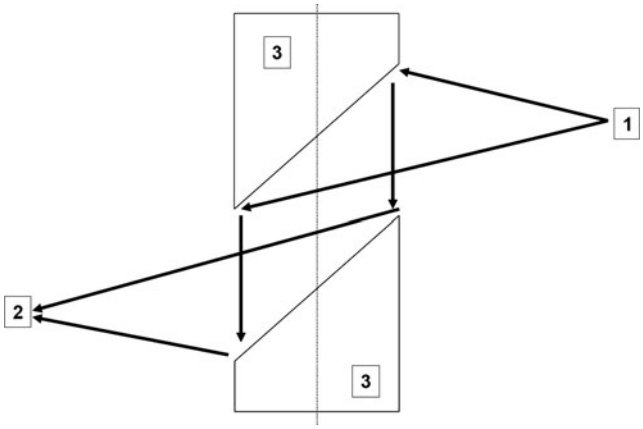

Fig. 3. Working scheme of parabolic-mirror-based light collection optics (not to scale), thick lines—show propagation of light in the system: (**1**) position of sample, (**2**) position of optical fiber, (**3**) parabolic off-axis mirrors.

product from Janos Technology Inc. (Keene, NH). The parabolic mirror condenser has a higher collection efficiency, however, it is more difficult to align, and has remarkable coma for probing areas with diameter greater than ≈ 0.5 mm. The spherical mirror system is less efficient but almost free from geometrical aberrations and more suitable for probing of larger areas. The fiber array consists of three 100 m long fibers (400 μm core, laboratory-grade, fused silica, low-OH, multi-mode, NA = 0.22) with fiber cores placed on one line oriented horizontally. It allows for simultaneous application of multiple instruments, e.g., pyrometer and spectrometers. Due to the 1:1 imaging of the optics, the probing area is equal to the diameter of the fiber core. In our experiments, we found 400 μm suitable both in terms of signal level and in terms of homogeneity of a sample's temperature distribution. For positioning and fine adjustment, the entire optical assembly is mounted on a motorized table that can be moved along the XYZ axes with better than 10 μm precision. The set-up is placed inside the vacuum chamber and can be controlled remotely.

Spectral Analyzer

The collected thermal light is coupled into the spectral analyzer (Fig. 4) *via* an SMA-905 fiber connector and discriminated at six wavelengths (channels). Two coated achromatic lenses ($f = 11$ mm and $f = 40$ mm) collimate the light into a quasi-parallel beam, which then undergoes successive reflections from six band pass interference filters. The mechanism of spectral resolution is based on the designed property of an interference filter being transparent for a narrow band of spectrum and acting as a mirror for the rest. The average peak transmission of the filters varies from 30% to 70%, depending on the center wavelength.

The wavelength selection is chosen to include the peak of the Planck curve, which shifts from near-infrared to visible during a temperature change from 2000 K to 10,000 K

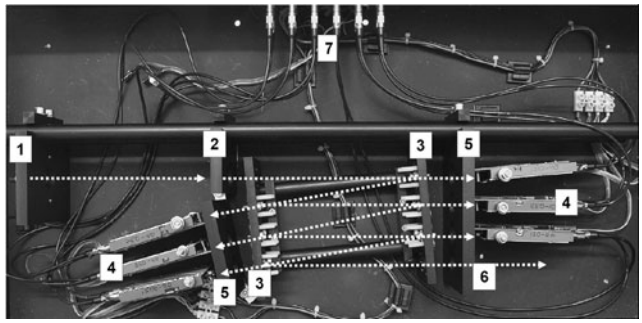

Fig. 4. Photograph and principal working scheme of the spectral analyzer, with the dashed lines showing propagation of light within instrument: (**1**) SMA-905 fiber coupling and 11 mm lens, (**2**) collimating $f = 40$ mm lens, (**3**) array of interference filters (six total), (**4**) photo detectors (six total), (**5**) final focusing $f = 18$ mm lenses (six total), (**6**) red diode laser, (**7**) outputs to digitizers.

(range expected in present experiments). The filters centered at 550, 750, 900, 1100, 1300, and 1500 nm, having widths of 40, 40, 40, 25, 25, and 20 nm, respectively. All filters are 1 inch in diameter and were purchased from the Andover Corporation (Salem, NH).

The mounting sequence of filters within the spectrometer was chosen to provide optimal signal levels at all channels simultaneously, taking into account the sensitivity of detectors and spectral intensity of the calibration source.

Interference filters are designed to work at the normal incidence, while in our arrangement the angle is $\approx 4.5^\circ$. The changes in transmission due to non-normal incidence were investigated using a laboratory spectrometer. The observed difference turned out to be about 0.2% shift of center wavelengths toward shorter wavelengths, which is small enough in comparison to the bandwidth of the filters.

The employed method of spectral discrimination is similar to the one proposed in Gardner *et al.* (1982) and has distinct advantages in terms of speed and efficiency, over conventional approaches, which include 45° beam splitters, time-multiplexed radiance onto a single detector using rotating filters, scanning spectrometer, etc. (Michalski *et al.*, 2001). The utilized approach gives the possibility of simultaneous analysis of the very same light beam at several wavelengths resulting in higher probing rates and no polarization dependence. Moreover, relatively low losses at each reflection allow for a higher number of channels.

At the final stage, the filtered light is focused by an $f =$ 18 mm aspherical lens to the detector consisting of a PIN photodiode connected to a custom trans-impendence current amplifier. With the given parameters of collimation and focusing optics of the spectral analyzer, the final spot size is smaller than the area of the detector. For fine positioning, the detector is mounted on a custom lockable kinematic stage. The fixation of the optics is stable and usually requires a single adjustment of optical components.

Two types of low-level dark-current photodiodes with 1 mm active area diameter are used: for channels from 550 nm to 900 nm, Si-diodes (Hamamatsu S7836-01), and

https://doi.org/10.1017/S0263034608000645 Published online by Cambridge University Press

for channels from 1100 nm to 1500 nm, InGaAs-diodes (Hamamatsu G8376-05). All detectors are operated in a biased, linear regime with a trans-impedance gain of 75 kV/A on a 50-Ω load and 5 ns rise in time. A conventional laboratory power supply provides 12 V of direct current (DC).

A red diode laser installed in the next free slot of the filter array and its position is adjusted so that its optical path is reverse to the propagation path of coupled light. The purpose of this laser is a quick check of the alignment of the filters in the array by measuring the laser power at the fiber input and comparing it with the value obtained during an optimal alignment of all filters.

The pyrometer is mounted in a chassis with an optical fiber input and electrical output ports at the outer panels. The modular design allows for swapping of various filters and detectors and can be upgraded to a higher number of channels.

Data Acquisition Hardware

Signal output of the pyrometer is recorded by a 24-channel, 8-bit digitizer (Acqiris DC271, 1 GHz bandwidth, 4 Gs/s) into a 50 Ω load with DC coupling with all inputs of the digitizer being synchronized to a picosecond. The acquisition is triggered using a TTL signal coming from the accelerator and tied to the arrival time of the ion beam at the target. The digitizer is controlled remotely from a PC over standard telecommunication optical fibers by means of a LabView code, which was developed for this purpose specifically. This code incorporates basic features of a conventional oscilloscope and allows for direct saving of data on a hard drive.

CALIBRATION

The pyrometer is calibrated (Michalski *et al.*, 2001; Dewitt, 1998) with a tungsten ribbon lamp of the "Pharaoh type," Osram W17/G powered by an ultra-stable DC power supply. The absolute radiation spectrum (2400 K at 650 nm) of a marked spot at the lamp's filament from 400 nm to 1600 nm (1 nm step) is provided by the manufacturer with 3% accuracy (Michalski *et al.*, 2001) (NIST traceable).

The continuous radiation of the lamp is modulated at 1 kHz by a mechanical chopper (removed during experiments) installed right after the fiber input to the spectral analyzer. For minimizing the noise of the calibration signal, the voltage values have been obtained from averaging over approximately 1000 acquisitions. Calibration is carried out with the very same components (condenser, vacuum feedthrough, optical fiber, etc.) as in the experiments, and already includes their optical transmission. During the calibration and data processing, transmission of the interference filter has been represented as Gaussian curves with FWHM corresponding to the documented width of the filters. Typical calibration voltages start from 10 mV for the shorter wavelength channels, and reach 200 mV for the near infrared channels. The typical saturation voltage of the detector into a 50 Ω load is $\approx \pm 4.5$ V with the noise level at ≈ 0.02 V root mean square. These numbers give rough estimations of lower and upper bounds of detectable blackbody temperatures determined by the noise level and the saturation voltage. For example, for the 550 nm channel, the detectable temperature range of a blackbody object is from 2400 K to 5000 K, while for the 1500 nm, it is from 1900 K to 9000 K. Higher temperatures can be measured by using an attenuation filter of known transmission. The usage of an attenuator will also shift the lower temperature bound toward higher values. Note that because the emissivity of an optically thick body in thermal equilibrium is normally less than one, the detectable physical temperature is generally higher than the blackbody temperature (Michalski *et al.*, 2001).

EXPERIMENTAL RESULTS

We demonstrate an experimental record of a tungsten target. In this experiment a freestanding tungsten foil, 100 μm thick, was pulse heated by an intense, focused ion beam, and eventually expanded hydrodynamically into vacuum (see Fig. 1). The U^{74+} beam was, 4×10^9 particles/bunch, 120 ns FWHM, had an elliptical profile (width ≈ 100 μm), and irradiated the entire sample.

The pyrometer was probing one side of the sample corresponding to a spot size of 400 μm, and was aimed at the quasi-homogenous region of the energy deposition curve (ion range in tungsten is ≈ 2 mm). Brightness temperatures measured in this experiment are plotted in Figure 5. In order to determine the physical temperature of the sample in the experiment, knowledge of both brightness temperature and spectral emissivity is required. When the emissivity in an experiment is not known, a way to approach the real value of temperature is to assume a plausible model (Coates, 1988; Pellerin *et al.*, 1992).

The employed pyrometer simultaneously measures the absolute radiation at multiple wavelengths, which gives an opportunity to apply various models of emissivity to experimental data at every point in time and to extract a temperature value from a non-linear least square fit (Coates, 1988).

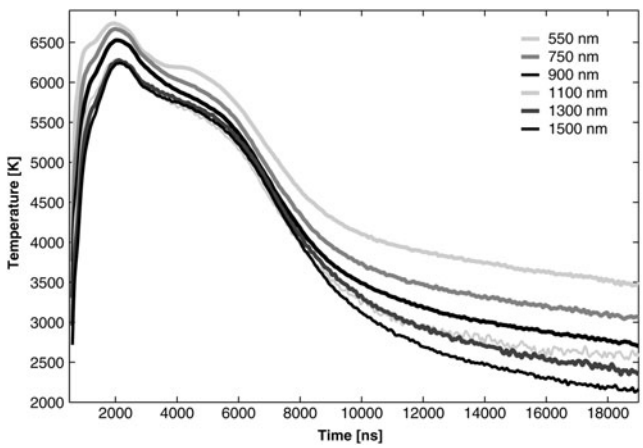

Fig. 5. Brightness temperatures of ion beam heated tungsten foil.

https://doi.org/10.1017/S0263034608000645 Published online by Cambridge University Press

Normally, the qualitative behavior of the emissivity in solid and cold liquid states is influenced by both surface conditions and optical constants of matter. In hot dense liquid and gaseous states, emissivity is governed mainly by the optical constants of the material, which are related to electrical conductivity of the medium, and once the conductivity is known, optical constants can be obtained in a straightforward way (Hagen & Rubens, 1903). The simplest and practical model of emissivity is based on the classical theory of conductivity proposed by Paul Drude in 1890. For example, it can be shown that there exists a wide range of wavelengths extending from the visible region up to the near-infrared region over which the emissivity of a solid and liquid metal to a good approximation, is constant (gray body) (Drude, 1904; Price, 1949). This approximation is widely applied to liquid metals in metallurgy, where a disordered state washes out much of the band structure, and the contribution of the specific conductive band is simplified (Michalski *et al.*, 2001; Celliers & Ng, 1993). The gray body model is also valid in the case of several highly reflective solid metals like polished aluminum and silver (Michalski, 2001) and also seems to be applicable in the density region around $1\,g/cm^3$. As it was shown in Celliers and Ng (1993), at this density value, the electronic structure is simple enough to be described by the Drude approximation. Such states appear, for example, during the release of a shocked metal.

Taking the above considerations into account, two empirical models of emissivity were applied in this work. The first one is the gray body approach as it is specifically justified for liquid and release states of WDM matter. The second model assumes a linear law of emissivity, which can be treated as a modified gray model with a linear term added. The linear model incorporates black and gray body cases and is a good approximation for some solid metals, e.g., tungsten (Dewitt, 1998).

In Figure 6, we show results of data processing for the two models with brightness temperatures at 550 nm and 1500 nm also plotted for a comparison. Figure 7 shows the actual fitting of these two models of radiation into experimental points at various moments of time. The temperature values

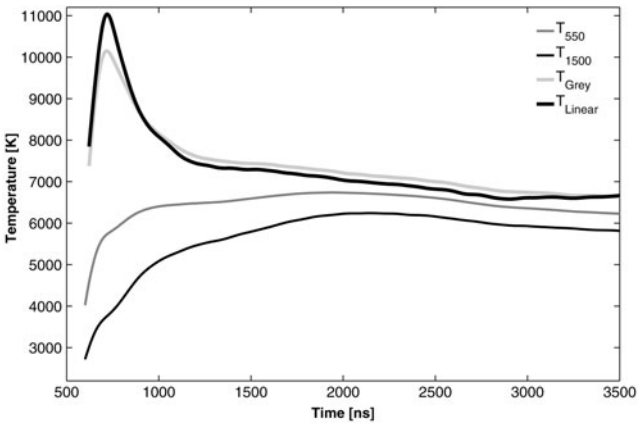

Fig. 6. Fitted temperatures obtained from the assumptions of gray or linear behavior of emissivity and brightness temperatures at 550 nm and 1500 nm.

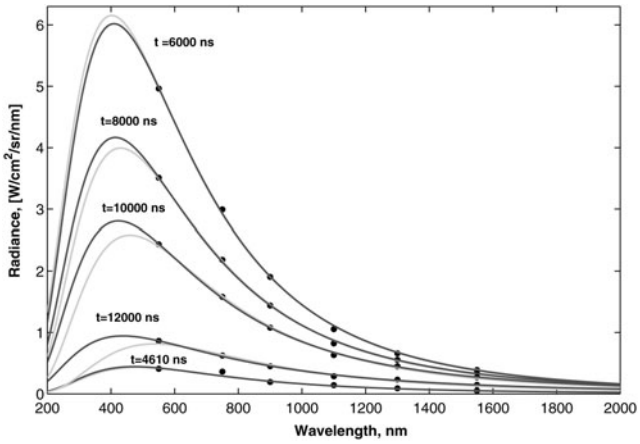

Fig. 7. Least-square fitting of experimental points (black circles) to radiation models with gray (gray) and linear (dark gray) behavior of emissivity at different moments of time.

demonstrated in these plots are only an estimation of reality and an attempt to reduce the effect of the unknown emissivity. However, their physical sense, in general, is debatable, and therefore should be considered only as a reference and as a supplement to the primary pyrometer output—brightness temperatures.

SUMMARY

A fast multichannel pyrometer has been designed and successfully commissioned in the recent WDM physics experiments with heavy ion beams. The pyrometer is a primary diagnostic tool in the present and future high energy-density physics experiments at GSI. A modification will be required, when the Facility for Antiproton and Ion Research (FAIR), the coming upgrade of GSI, will be operational, where higher and faster heating rates are expected. The instrument is designed such that an upgrade toward higher temperatures and higher speed can be carried out rather easily; components satisfying future regimes are available now. The new experimental data, developed diagnostics and experience gained from this work are also of great importance for planning future WDM physics experiments at FAIR (Hoffmann *et al.*, 2005; Henning, 2004; Tahir *et al.*, 2007*b*).

ACKNOWLEDGMENTS

The authors wish to thank D. Fernengel, J. Menzel, and H. Wahl for their help in preparing the experiments. This work has been supported in part by the GSI-INTAS grants 03-54-4254.

REFERENCES

Adonin, A., Jacoby, J., Turtikov, V., Fertman, A., Golubev, A., Hoffmann, D.H.H., Ulrich, A., Varentsov, D. & Wieser, J. (2007). Laser effect on the 248 nm KrF transition using heavy ion beam pumping. *Nucl. Instrum. & Meth. Phys. Res. A* **577**, 357–360.

https://doi.org/10.1017/S0263034608000645 Published online by Cambridge University Press

Becker, F., Hug, A., Forck, P., Kulish, M., Ni, P., Udrea, S. & Varentsov, D. (2006). Design, development, and testing of non-intercepting profile diagnostics for intense heavy ion beams using a capacitive pickup and beam induced gas fluorescence monitors. *Laser Part. Beams* **24**, 541–551.

Cao, L.F., Uschmann, I., Zamponi, F., Kampfer, T., Fuhrmann, A., Forster, E., Holl, A., Redmer, R., Toleikis, S., Tschentscher, T. & Glenzer, S.H. (2007). Space-time characterization of laser plasma interactions in the warm dense matter regime. *Laser Part. Beams* **25**, 239–244.

Celliers, P. & Ng, A. (1993). Optical probing of hot expanded states produced by shock release. *Phys. Rev. E* **47**, 3547–3565.

Coates, P.B. (1988). The least-squares approach to multi-wavelength pyrometry. *High Temp. High Pressure* **20**, 433–441.

Deutsch, C. & Popoff, R. (2006). Low velocity ion stopping of relevance to the US beam-target program. *Laser Part. Beams* **24**, 421–425.

Dewitt, D.P. (1998). *Theory and Practice of Radiation Thermometry*. New York: John Wiley & Sons.

Drude, P. (1904). Optische Eigenschaften und Elektronentheorie. *Annalen der Physik* **319**, 677–725.

Fortov, V.E., Ilkaev, R.I., Arinin, V.A., Burtzev, V.V., Golubev, V.A., Iosilevskiy, I.L., Khrustalev, V.V., Mikhailov, A.L., Mochalov, M.A., Ternovoi, V.Y. & Zhernokletov, M.V. (2007). Phase transition in a strongly nonideal deuterium plasma generated by quasi-isentropical compression at megabar pressures. *Phys. Rev. Lett.* **99**.

Gardner, J.L., Jones, T.P. & Sainty, W.G. (1982). Induced-transmission interference-filter array for multiwavelength pyrometry. *Appl. Opt.* **21**, 1259–1261.

Hagen, E. & Rubens, H. (1903). Über die Beziehungen des Reflexions- und Emissionsvermögens der Metalle zu ihrem elektrischen Leitvermögen. *Annalen der Physik* **11**, 873–901.

Henning, W.F. (2004). The future GSI facility. *Nucl. Instrum. & Meth. Phys. Res. B* **214**, 211–215.

Hoffmann, D.H.H., Blazevic, A., Korostiy, S., Ni, P., Pikuzc, S.A., Rethfeld, B., Rosmej, O., Roth, M., Tahir, N.A., Udrea, S., Varentsov, D., Weyrich, K., Sharkov, B.Y. & Maron, Y. (2007). Inertial fusion energy issues of intense heavy ion and laser beams interacting with ionized matter studied at GSI-Darmstadt. *Nucl. Instrum. & Meth. Phys. Res. A* **577**, 8–13.

Hoffmann, D.H.H., Blazevic, A., Ni, P., Rosmej, O., Roth, M., Tahir, N.A., Tauschwitz, A., Udrea, S., Varentsov, D., Weyrich, K. & Maron, Y. (2005). Present and future perspectives for high energy density physics with intense heavy ion and laser beams. *Laser Part. Beams* **23**, 47–53.

Hora, H. (2007). New aspects for fusion energy using inertial confinement. *Laser Part. Beams* **25**, 37–45.

Logan, B.G., Bieniosek, F.M., Celata, C.M., Coleman, J., Greenway, W., Henestroza, E., Kwan, J.W., Lee, E.P., Leitner, M., Roy, P.K., Seidl, P.A., Vay, J.L., Waldron, W.L., Yu, S.S., Barnard, J.J., Cohen, R.H., Friedman, A., Grote, D.P., Covo, M.K., Molvik, A.W., Lund, S.M., Meier, W.R., Sharp, W., Davidson, R.C., Efthimion, P.C., Gilson, E.P., Grisham, L., Kaganovich, I.D., Qin, H., Sefkow, A.B., Startsev, E.A., Welch, D. & Olson, C. (2007). Recent US advances in ion-beam-driven high energy density physics and heavy ion fusion. *Nucl. Instrum. & Meth. Phys. Res. A* **577**, 1–7.

Michalski, L., Eckersdorf, K., Kucharski, J. & McGhee, J. (2001). *Temperature Measurement*. New York: John Wiley & Sons.

Mitchell, A.C., Nellis, W.J., Moriarty, J.A., Heinle, R.A., Holmes, N.C., Tipton, R.E. & Repp, G.W. (1991). Equation of state of Al, Cu, Mo, and Pb at shock pressures up to 2.4 Tpa (24-Mbar). *J. Appl. Phys.* **69**, 2981–2986.

Pellerin, M.A., Tsai, B.K., Dewitt, D.P. & Dall, G.J. (1992). *Temperature, Its Measurement and Control in Science and Industry*. College Parks, MD: American Institute of Physics.

Price, D.J. (1949). A theory of reflectivity and emissivity. *Proc. Phys. Soc. A* **62**, 278–283.

Sasaki, T., Yano, Y., Nakajima, M., Kawamura, T. & Horioka, K. (2006). Warm-dense-matter studies using pulse-powered wire discharges in water. *Laser Part. Beams* **24**, 371–380.

Tahir, N.A., Adonin, A., Deutsch, C., Fortov, V.E., Grandjouan, N., Geil, B., Grayaznov, V., Hoffmann, D.H.H., Kulish, M., Lomonosov, I.V., Mintsev, V., Ni, P., Nikolaev, D., Piriz, A.R., Shilkin, N., Spiller, P., Shutov, A., Temporal, M., Ternovoi, V., Udrea, S. & Varentsov, D. (2005*a*). Studies of heavy ion-induced high-energy density states in matter at the GSI Darmstadt SIS-18 and future FAIR facility. *Nucl. Instrum. & Meth. Phys. Res. A* **544**, 16–26.

Tahir, N.A., Deutsch, C., Fortov, V.E., Gryaznov, V., Hoffmann, D.H.H., Kulish, M., Lomonosov, I.V., Mintsev, V., Ni, P., Nikolaev, D., Piriz, A.R., Shilkin, N., Spiller, P., Shutov, A., Temporal, M., Ternovoi, V., Udrea, S. & Varentsov, D. (2005*b*). Proposal for the study of thermophysical properties of high-energy-density matter using current and future heavy-ion accelerator facilities at GSI Darmstadt. *Phys. Rev. Lett.* **95**, 035001.

Tahir, N.A., Piriz, A.R., Shutov, A., Varentsov, D., Udrea, S., Hoffmann, D.H.H., Juranek, H., Redmer, R., Portugues, R.F., Lomonosov, I. & Fortov, V.E. (2003). The creation of strongly coupled plasmas using an intense heavy ion beam: Low-entropy compression of hydrogen and the problem of hydrogen metallization. *J. Phys. A* **36**, 6129–6135.

Tahir, N.A., Schmidt, R., Brugger, M., Lomonosov, I.V., Shutov, A., Piriz, A.R., Udrea, S., Hoffmann, D.H.H. & Deutsch, C. (2007*a*). Prospects of high energy, density physics research using the CERN super proton synchrotron (SPS). *Laser Part. Beams* **25**, 639–647.

Tahir, N.A., Spiller, P., Shutov, A., Lomonosov, I.V., Gryaznov, V., Piriz, A.R., Wouchuk, G., Deutsch, C., Fortov, V.E., Hoffmann, D.H.H. & Schmidt, R. (2007*b*). HEDgeHOB: High-energy density matter generated by heavy ion beams at the future facility for antiprotons and ion research. *Nucl. Instrum. & Meth. Phys. Res. A* **577**, 238–249.

Udrea, S., Ternovoi, V., Shilkin, N., Fertman, A., Fortov, V.E., Hoffmann, D.H.H., Hug, A., Kulish, M.I., Mintsev, V., Ni, P., Nikolaev, D., Tahir, N.A., Turtikov, V., Varentsov, D. & Yuriev, D. (2007). Measurements of electrical resistivity of heavy ion beam produced high energy density matter: Latest results for lead and tungsten. *Nucl. Instrum. & Meth. Phys. Res. A* **577**, 257–261.

Varentsov, D., Tahir, N.A., Lomonosov, I.V., Hoffmann, D.H.H., Wieser, J. & Fortov, V.E. (2003). Energy loss dynamics of an intense uranium beam interacting with solid neon for equation-of-state studies. *Europhys. Lett.* **64**, 57–63.

Varentsov, D., Ternovoi, V.Y., Kulish, M., Fernengel, D., Fertman, A., Hug, A., Menzel, J., Ni, P., Nikolaev, D.N., Shilkin, N., Turtikov, V., Udrea, S., Fortov, V.E., Golubev, A.A., Gryaznov, V.K., Hoffmann, D.H.H., Kim, V., Lomonosov, L., Mintsev, V., Sharkov, B.Y., Shutov, A.,

Spiller, P., Tahir, N.A. & Wahl, H. (2007). High-energy-density physics experiments with intense heavy ion beams. *Nucl. Instrum. & Meth. Phys. Res. A* **577**, 262–266.

Weir, S.T., Mitchell, A.C. & Nellis, W.J. (1996). Metallization of fluid molecular hydrogen at 140 GPa (1.4 mbar). *Phys. Rev. Lett.* **76**, 1860–1863.

Zou, X.B., Liu, R., Zeng, N.G., Han, M., Yuan, J.Q., Wang, X.X. & Zhang, G.X. (2006). A pulsed power generator for x-pinch experiments. *Laser Part. Beams* **24**, 503–509.

Zvorykin, V.D., Didenko, N.V., Ionin, A.A., Kholin, I.V., Konyashchenko, A.V., Krokhin, O.N., Levchenko, A.O., Mavritskii, A.O., Mesyats, G.A., Molchanov, A.G., Rogulev, M.A., Seleznev, L.V., Sinitsyn, D.V., Tenyakov, S.Y., Ustinovskii, N.N. & Zayarnyi, D.A. (2007). GARPUN-MTW: A hybrid Ti:Sapphire/KrF laser facility for simultaneous amplification of subpicosecond/nanosecond pulses relevant to fast-ignition ICF concept. *Laser Part. Beams* **25**, 435–451.

https://doi.org/10.1017/S0263034608000645 Published online by Cambridge University Press